
TRACKING AND LONG-TERM IDENTIFICATION USING NON-VISUAL MARKERS

UNDER REVIEW

Michael P. J. Camilleri
School of Informatics,
University of Edinburgh

Li Zhang
School of Data Science,
Fudan University

Rasneer S. Bains
Mary Lyon Centre,
MRC Harwell

Andrew Zisserman
Dept. of Engineering Science,
University of Oxford

Christopher K. I. Williams
School of Informatics
University of Edinburgh

ABSTRACT

Our objective is to track and identify mice in a cluttered home-cage environment, as a precursor to automated behaviour recognition for biological research. This is a very challenging problem due to (i) the lack of distinguishing visual features for each mouse, and (ii) the close confines of the scene with constant occlusion, making standard visual tracking approaches unusable. However, a coarse estimate of each mouse’s location is available from a unique RFID implant, so there is the potential to optimally combine information from (weak) tracking with coarse information on identity.

To achieve our objective, we make the following key contributions: (a) the formulation of the *identification* problem as an assignment problem (solved using Integer Linear Programming), and (b) a novel probabilistic model of the affinity between tracklets and RFID data. The latter is a crucial part of the model, as it provides a principled probabilistic treatment of object detections given coarse localisation. Our approach achieves 77% accuracy on this identification problem, and is able to reject spurious detections when the animals are hidden.

1 Introduction

We are motivated by the problem of tracking group-housed mice in a cluttered home-cage environment, as in Fig. 1. The *identification* problem goes beyond tracking to assigning unique identities to each animal, as a precursor to automatically annotating their individual behaviour (e.g., feeding, grooming) in the video, and analysing their interactions. The mice have no distinguishing visual features, making standard visual tracking approaches very difficult when the mice are huddled or interacting together. This difficulty is compounded by the close confines of the enriched cage environment. However, we can leverage additional information provided by a unique Radio-Frequency Identification (RFID) implant in each mouse, to provide a coarse estimate of its location (on a 3×6 grid). This setting is not unique to animal tracking. Similar situations arise e.g., when identifying specific team-mates in robotic soccer [1] (where the identification is provided by the weak self-localisation of each robot), or identifying vehicles observed by traffic cameras at a busy junction (as required for example for law-enforcement), making use of a weak location signal provided by cell-phone data.

Our solution starts from training and running a mouse detector on each frame, and grouping the detections together with a tracker [2] to produce a set of tracklets, as shown in Fig. 2(c). We then formulate an assignment problem to *identify* each tracklet as belonging to a mouse (based on RFID data) or a dummy object (to capture spurious tracklets). This problem is solved using Integer Linear Programming (ILP), see Fig. 2(f). Tracking is used to reduce the complexity of the problem relative to a frame-wise approach and implicitly enforce temporal continuity for the solution.

The problem setup is not standard Multi-Object Tracking (MOT), since we go beyond tracking by *identifying* individual tracklets using additional RFID information which provides persistent unique identifiers for each animal. Our

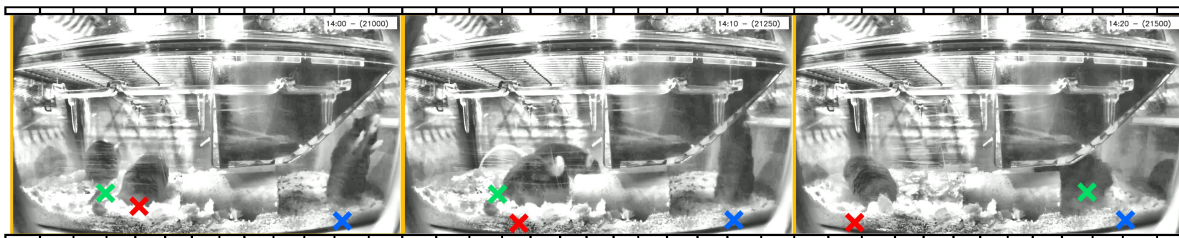


Figure 1: Sample frames from our dataset. To improve visualisation, the frames are processed with CLAHE [4] and brightened: our methods operate on the raw frames. The mice are visually indistinguishable, their identity being inferred through the RFID pickup, shown as Red/Green/Blue crosses projected into image-space. This is enough to distinguish the mice when they are well separated (left): however, as they move around, they are occluded by cage elements (Green in centre) or by cage mates (Green by Blue in right) and we have to reason about temporal continuity and occlusion dynamics.

main contribution is thus to formulate this *identification* as an assignment problem, and solve it using ILP. A key part of the model is a principled probabilistic treatment for modelling detections from the coarse localization information, which is used to provide assignment weights to the ILP. Finally we emphasize that we are solving a real-world problem which is of considerable importance to the biological community (International Mouse Phenotype Consortium (IMPC), [3]), and which needs to scale up to thousands of hours of data in an efficient manner — this necessarily affects some of our design choices.

In this paper we first frame our problem in light of recent efforts (§2, indicating how our situation is quite unique in its formulation. We discuss our approach from a theoretical perspective in §3, postponing the implementation details to §4. Finally, we showcase the utility of our solution through rigorous experiments (§5) which allows us to analyse its merits in some depth. Details for replicating our experimental setups (including parameter fine-tuning) as well as deeper theoretical insights is relegated to the Supplementary Material. We also released our code together with some video clips of our framework in action at <https://github.com/michael-camilleri/TIM>.

2 Related work

Below we discuss related work w.r.t. MOT, re-identification (re-ID) and animal tracking. We defer discussion of our ILP formulation relative to other work after discussing the method in §3.2.

Multi-Object Tracking: There have been many recent advances in MOT [5], fuelled in part by the rise of specialised neural architectures [6, 7, 8]. Here the main challenge is keeping track of an undefined number of *visually distinct* objects (often people, as in e.g. [9, 10]), over a short period of time (as they enter and exit a particular scene) [11]. However, our problem is not MOT because we need to *identify* (rather than just track) a fixed set of individuals using persistent, externally-assigned identities, rather than relative ones (as in e.g. [12]): i.e. our problem is not indifferent to label-switching. We care about the absolute identity assigned to each tracklet – even if we had input from a perfect tracker, there would still need to be a way to assign the anonymous tracklets to identities, as we do below.

There is another important difference between the current state of the art (SOTA) in MOT (see e.g. [13, 7, 14, 15, 12, 16, 17]) and our use-case. As the mice are essentially indistinguishable, we cannot leverage appearance information to distinguish them but must rely on external cues – the RFID-based quantised position. On top of this, there are also the challenges of operating in a constrained cage environment (which exacerbates the level of occlusion), and the need to consistently and efficiently track mice over an extended period of time (on the order of hours).

(Re-)Identification: Re-ID [18] addresses the transitory notion of identity by using appearance cues to join together instances of the same object across ‘viewpoints’. Obviously, this does not work when objects are visually indistinguishable, but there is also another key difference. The standard re-ID setup deals with associating together instances of the same object, often (but not necessarily) across multiple non-overlapping cameras/viewpoints [19]. In our specific setup, however, we wish to relate objects to an external identity (e.g. RFID-based position); our work thus sits on top of any algorithm that builds tracklets (such as that of Fleuret et al. [18]).

Animal Tracking: Our unique setup is significantly more challenging than traditional animal observation models, which side-step identification by involving single animals in a purpose-built arena [20, 21, 22, 23] rather than our enriched home-cage. Recent work on multiple-animal tracking often uses visual features for identification [14, 24]

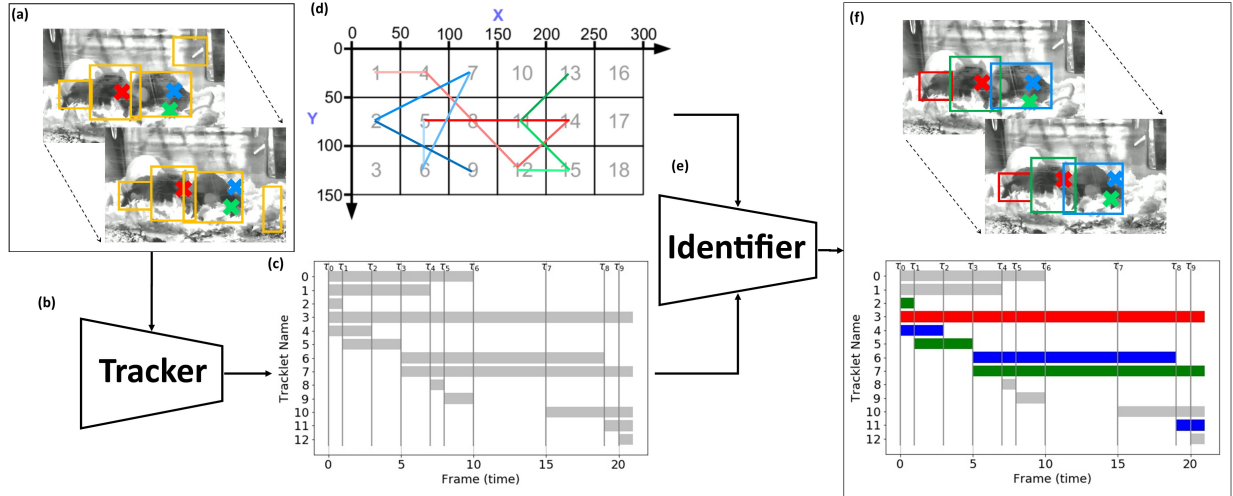


Figure 2: Our proposed architecture. Given per-frame detections of animals (a), a tracker (b) joins these into tracklets, shown (c) in terms of their temporal span. After discarding spurious detections based on a lifetime threshold, the identifier (e) combines these with coarse localisation traces over time (d), to produce identified Bounding Boxes (BBs) for each object throughout the video, shown (f) as coloured tracklets/BBs.

which we cannot leverage, requires access to richer sources of colour/depth information [25, 26] rather than our single-channel Infra-Red (IR) feed, or employs top-mounted cameras [26, 27, 28, 29, 14] which give a much less cluttered view of the animals. Indeed, systems such as idtracker.ai [30] or DeepLabCut [31] do not work for our setup, since the mice often hide each other and keypoints on the animals (which are an integral part of the methods) are not consistently visible (besides requiring more onerous annotations).

3 Methodology

This section describes our proposed approach to identification of a fixed set of objects from a theoretical perspective. Implementation details are deferred to section §4. We explain the methodology through the running example of tracking group-housed animals.

Overview: Our system takes in candidate detections about a fixed set of animals in the form of Bounding Boxes (BBs) and assigns an identity to each of them using a two-stage pipeline, as shown in Fig. 2. First, we use a *Tracker* [2] to join the detections across frames into tracklets based on optimising the Intersection-over-Union (IoU) between Bounding Boxes (BBs) in adjacent frames. This stage injects temporal continuity into the identification, filters out spurious detections, and, as will be seen later, reduces the complexity of the identification problem. Then, an *Identifier*, using a novel ILP formulation, combines the tracklets with the coarse position information to identify which tracklet(s) belong to each of the known animals, based on a probabilistic weight model of object locations.

3.1 Tracking

We use the tracker to inject temporal continuity into our problem, encoding the prior that animals can only move a limited distance between successive frames. Subsequently, we formulate our identification problem as assigning *tracklets* to animals over a recording interval indexed by $t \in \{1, \dots, T\}$.

The tracker also serves the purpose of simplifying the optimisation problem. While BBs and positions are registered at the video frame rate, it is not necessary to run our optimisation problem (below) at this granularity. Rather, we group together the sequence of frames for which the same subset of tracklets are visible: a new interval will begin when a new tracklet is spawned, or when an existing one disappears. The observation is thus broken up into intervals, indexed sequentially by t , shown as $\tau_{\{0, \dots, 9\}}$ at the top of Fig. 2 (c).

3.2 Identification from tracklets

The tracker produces I tracklets: to this we add T special ‘hidden’ tracklets for which no BBs exist, and which serve to model occlusion at any time-step. The goal of the Identifier is then to assign object identities to the set of tracklets, S , of size $I + T$. The set of tracklets visible at time t is represented by L_t . We assume there are J animals o_1, \dots, o_J we wish to track/identify (and for which we have access to coarse location through time); an extra dummy object o_{J+1} is a special outlier/background model which captures spurious tracklets in S .

We also define a utility w_{ij} , which is a measure of the quality of the match between tracklet s_i and animal o_j : we assume that tracklets cannot switch identities and are assigned in their entirety to one animal (this is reasonable if we are liberal in breaking tracklets). The weight is typically a function of the BB features and animal position (see §3.3). Given the above, our ILP optimises the assignment matrix A with elements $a_{ij} \in \{0, 1\}$ (where $a_{i,j} = 1 \Leftrightarrow 's_i$ is assigned to o_j'), that maximises:

$$\max_A \sum_{i=1}^{I+T} \sum_{j=1}^{J+1} w_{ij} a_{ij}, \quad (1)$$

subject to the constraints:

$$\sum_{j=1}^{J+1} a_{ij} = 1 \quad \forall i \in I, \quad (2)$$

$$\sum_{l \in L_t} a_{lj} = 1 \quad \forall t \in T, j \in J, \quad (3)$$

$$a_{iJ+1} = 0 \quad \forall I + 1 \leq i \leq I + T. \quad (4)$$

Constraint (2) ensures that a *generated* tracklet is assigned to exactly one animal, which could be the outlier model. Constraint (3), enforces that each animal (excluding the outlier model) is assigned exactly one tracklet (which could be the ‘hidden’ tracklet) at any point in time, and finally, Eq. (4) prevents assigning the hidden tracklets to the outlier model. Unfortunately, these constraints mean that the resulting linear program is not Totally Unimodular [32], and hence does not automatically yield integral optima. Consequently, solving the ILP is in general NP-Hard, but we have found that due to our temporal abstraction, using a branch and cut approach efficiently finds the optimal solution on the size of our data without the need for any approximations.

Our ILP formulation of the Identification process is related to the general family of covering problems [33] as we show in our Supplementary Material (see §B.1). In this respect, our problem is a generalisation of Exact-Set-Cover [34] in that we require every animal to be ‘covered’ by one tracklet at each point in time: i.e. we use the stronger equality constraint rather than the inequality in the general ILP (see Eq. (B.2)). Unlike the Exact-Set-Cover formulation, however, (a) we have multiple objects (animals) to be covered, (b) some objects need not be covered at all (outlier model), *and* (c) all detected tracklets must be used (although a tracklet can cover the ‘extra’ outlier model). Note that with respect to (a), this is not the same as Set Multi-Cover [35] in which the same object must be covered more than once: i.e. Eq. (B.2) is always 1 for us.

3.3 Assignment weighting model

The weight matrix with elements w_{ij} is the essential component for incorporating the quality of the match between tracklets and locations. It is easier to define the utility of assignments on a per-frame basis, aggregating these over the lifetime of the tracklet. The per-frame weight boils down to the level of agreement between the features of the BB and the position of the object at that frame, together with the presence of other occluders.

We can use any generative model for this purpose, with the caveat that we can only condition the observations (BBs) on fixed information which does not itself depend on the result of the ILP assignment. Specifically, we can use all the RFID information and even the presence of the tunnel, but not the locations of other BBs. The reason for this is that if we condition on the other detections, the weight will depend on the other assignments (e.g. whether a BB is assigned to a physical object or not), which invalidates the ILP formulation.

We define our weight model as the probability that an animal picked up by a particular RFID antenna j , or the outlier distribution $J + 1$, could have generated the BB i . For the sake of our ILP formulation, we also allow animal j to generate a hidden BB when it is not visible.

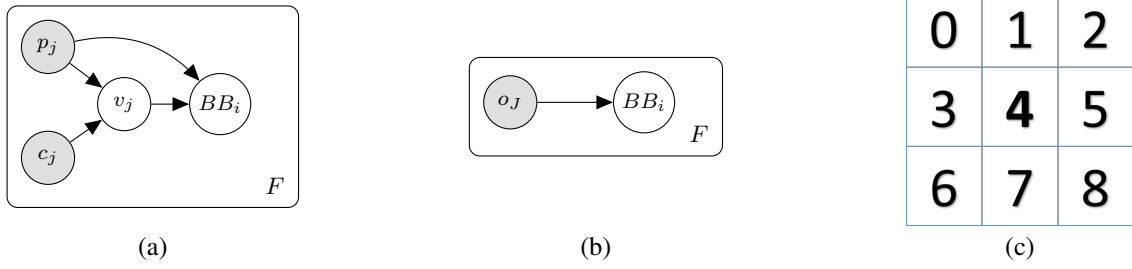


Figure 3: (a) Model for assigning BB_i to o_j (per-frame in F) when o_j is an animal. Variable p_j refers to the position of animal j , and c_j captures contextual information. The visibility is represented by v_j , and the BB (actual or occluded) by BB_i . (b) Model for assigning BB_i under the outlier model. (c) Neighbourhood definition for representing c_j .

For objects of interest ($j \leq J$), we employ the graphical model Fig. 3 (a). Variable p_j represents the position of object j ; c_j captures contextual information, which impacts the visibility v_j of the BB and is a function of the RFID pickups of the other animals in the frame. v_j can take on one of three values: (1) clear (fully visible), (2) truncated (partial occlusion), and (3) hidden (object is fully occluded and hence no BB appears for it). The BB parameters are then conditioned on both the object position (for capturing the relative arrangement within the observation area) as well as the visibility as:

$$P(BB_i | p_j, v_j) \sim \begin{cases} 1 & \text{if } v_j = \text{Hidden} \ \& \ i \geq I + 1 \\ 0 & \text{if } v_j = \text{Hidden} \ \& \ i < I + 1, \\ \mathcal{N}(\mu_{pv}, \Sigma_{pv}) & \text{otherwise} \end{cases}, \quad (5)$$

where the parameters of the Gaussian are in general a function of object position and visibility. Note that in the top line of Eq. (5) we allow only a hidden object to generate a ‘hidden’ tracklet. Conversely, under the outlier model, Fig. 3 (b), the BB is modelled as a single broad distribution, capturing the probability of having spurious detections.

Bringing it all together, the *per-frame* weight, $w_{i,j}^{(f)} = \log P(BB_i^{(f)} | p_j^{(f)}, c_j^{(f)})$, with

$$P(BB_i | p_j, c_j) = \begin{cases} \sum_{v_j} P(BB_i | p_j, v_j) P(v_j | p_j, c_j) & \text{if } j < J + 1 \\ P(BB_i | o_j) & \text{otherwise} \end{cases}, \quad (6)$$

where we have dropped the frame index for clarity. The complete tracklet-object weight $w_{i,j}$ is then the sum of the log-probabilities over the tracklet’s visible lifetime.

3.4 Relation to other methods

A number of works (see e.g. [36, 18, 37, 38]) have used ILP to address the tracking problem, however we reiterate that our task goes beyond tracking to data association with the external information. Indeed, in all of the above cited approaches, the emphasis is on joining the successive detections into contiguous tracklets, while our focus is on the subsequent step of identifying the tracklets by way of the RFID position.

Solving identification problems similar to our is typically achieved through hypothesis filtering, e.g. Joint Probabilistic Data Association (JPDA) [36]. While we could have posed our problem into this framework (which would be a contribution in its own right, with the inclusion of the position-affinity model in §3.3), exact inference for such a technique increases exponentially with time. While there are approximation algorithms (e.g. [39]), our ILP formulation: (a) does not explicitly model temporal continuity (by delegating this to the tracker), (b) imposes the restriction that the (per-frame) weight of an animal-tracklet pair is a function only of the pair (i.e. independent of the other assignments), (c) estimates a *Maximum-A-Posteriori* (MAP) tracklet weight rather than maintaining a global distribution over all possible tracklets, *but then* (d) optimises for a globally consistent solution rather than running online frame-by-frame filtering. The combination of (a), (b) and (c) greatly reduce the complexity of the optimisation problem compared to JPDA, allowing us to optimise an offline global assignment (d) without the need for simplifications/approximations.

4 Implementation details

4.1 Detector

We use the object detector FCOS [40] with a ResNet-50 [41] backbone, although our method is agnostic to the type of detector as long as it outputs BBs. We replace the classifier layer of the pre-trained network with three categories (i.e., *mouse*, *tunnel* and *background*) and fine-tune the model on our data (see Supplementary Material §C.1). In the final configuration, we accept all detections with confidence above 0.4, up to a maximum of 5 per image. We further discard BBs which fall inside the hopper area by thresholding on a maximum ratio of overlap (with hopper) to BB area of 0.4. This setup achieves a recall (at IoU=0.5) of 0.90 on the held-out test-set (average precision is 0.87, CoCo Mean Average Precision (mAP)=0.60).

4.2 Tracker

We use the SORT tracker of Bewley et al. [2] which maintains a ‘latent’ state of the tracklet (the centroid (x, y) of the BB, its area and the aspect ratio, together with the velocities for all but the aspect ratio) and assigns new detections in successive frames based on IoU. At each frame, the state of each active tracklet is updated according to the Kalman predictive model, and new detections matched to existing tracklets by the Hungarian algorithm [2] on the IoU (subject to a cutoff).

Our plug’n’play approach would allow us to use other advanced trackers (e.g. [42, 8, 37, 43]), but we chose this tracker for its simplicity. Since most of the above methods leverage visual appearance information, and all mice are visually similar, it is likely that any marginal improvements would be outweighed by a bigger impact on scalability. In addition, previous research (e.g. [11]) has shown that simple methods often outperform more complex ones, but we leave experimentation with trackers as possible future research.

We do, however, make some changes to the architecture, in light of the fact that we do not need online tracking, and hence can optimise for retrospective filtering. The first is that tracklets emit BBs from the start of their lifetime, and we do not wait for them to be active for a number of frames: this is because, we can always filter our spurious detections at the end. Secondly, when filtering out short tracklets, we do this based on a minimum number of contiguous (rather than total) frames — again, we can do this because we have access to the entire lifetime of each tracklet. We also opt to emit the original detection as the BB rather than a smoothed trajectory, since we believe that the current model assuming a fixed aspect ratio might be too restrictive for our use-case — indeed, we plan to experiment with different models for the Kalman state in the future. Finally, we take the architectural decision to kill tracklets as soon as they fail to capture a detection in a frame: our motivation is that we prefer to have broken tracklets which we can join later using the identification rather than increasing the probability of a tracklet switching identity.

To optimise the two main parameters of the tracker — the IoU threshold for assigning new detections to existing tracklets, and the minimum lifetime of a tracklet to be considered viable — we used the combined training/validation set, and ran our ILP identification end-to-end over a grid of parameters. The optimal results were obtained using a length cutoff of 2 frames and IoU threshold of 0.8 (see Supplementary Material §C.2 for details).

4.3 Weight model

We represent BBs by the 4-vector containing the centroid $[x, y]$ and size $[width, height]$ of the axis-aligned BB. A hidden BB is denoted by the zero-vector and is handled explicitly in logic. The visibility, v_j can be one of clear, truncated or hidden as already discussed, while the position, p_j is an integer representing the one-of-18 antennas in which the mouse is picked up. For c_j we consider the RFID pickups of the other two mice, but we must represent them in an (identity) permutation-invariant way: i.e. the representation must be independent of the identify of the animal we are predicting for (all else being equal). To this end, we define a nine-point neighbourhood around the antenna p_j as in Fig. 3(c), where p_j would fall in cell 4. Note that where the neighbourhood extends beyond the range of the antenna base-plate, these cells are simply ignored. c_j is then simply the count of animals picked up in each cell (0, 1 or 2).

Under the outlier model (Fig. 3 (b)), the BB centroids, $[x, y]$, are drawn from a very wide Gaussian over the size of the image: the size, $[w, h]$ is Gaussian with its mean and covariance fit on the training/validation annotations. For the non-outlier case (Fig. 3(a)) we model the distribution $p(v_j|p_j, c_j)$ using a Random Forest (RF): this proved to be the best model in terms of validation log-likelihood (this metric is preferable for a calibrated distribution). The mean μ_{pv} of the multivariate Gaussian for the BB parameters at position p with visibility v in Eq. (5) is defined as follows. The centroid components $[x, y]$ are the same irrespective of the visibility, and governed by a homography mapping between the antenna positions on the ground-plane and the annotated BBs centroids in the image. The width and height, $[w, h]$ are estimated independently for each row in the antenna arrangement (see Fig. 1 (b)) and visibility (clear/truncated).

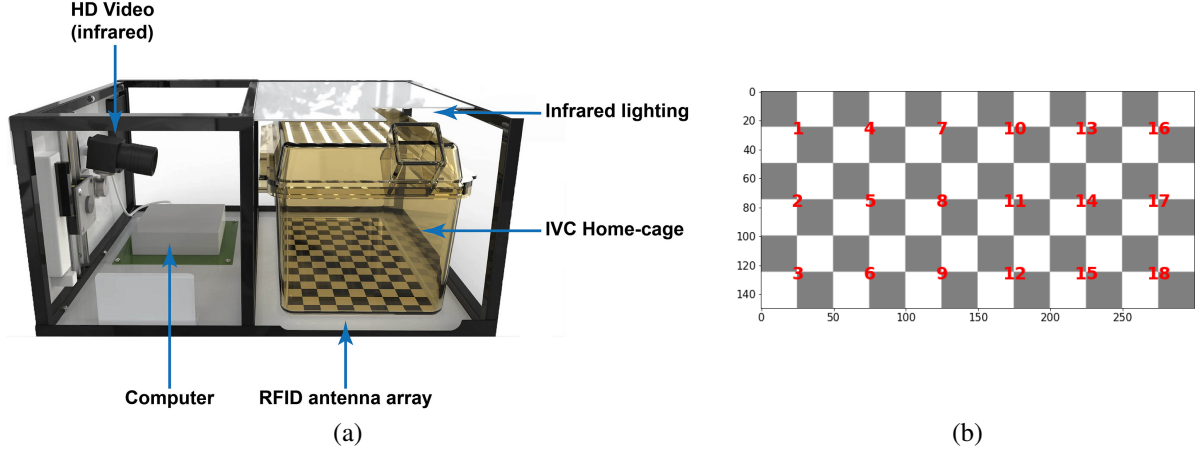


Figure 4: The Actual Analytics Home Cage Analysis system. (a) The rig used to capture mouse recordings (Illustration reproduced with permission from [47]). (b) The (numbered) points on the checkerboard pattern used for calibration (measurements are in mm): the numbers correspond also to the RFID antenna receivers on the baseplate.

This models occlusion and perspective projection but allows us to pool samples across pickups for statistical strength. The covariance matrix Σ_{pv} is estimated solely on a per-row basis, and is independent of the visibility. Further details on fine-tuning the parameters appear in our Supplementary Material (§C.3).

4.4 Solver

Unfortunately, our linear program is not Totally Unimodular [32] due to the constraints in Eqs. (2 – 4), and hence, we have to explicitly enforce integrality. Consequently, solving the ILP is in general NP-Hard, but we have found that due to our temporal abstraction, using a branch and cut approach efficiently finds the optimal solution on the size of our data. We model our problem through the Python MIP package [44], using the COIN-OR Branch and Cut [45] paired with the COIN-OR Linear Programming [46] solvers. Running on a conventional desktop (Intel Xeon E3-1245 @3.5GHz with 32Gb RAM), the solver required on the order of a minute on average for each 30-minute segment.

5 Experiments

5.1 Dataset

Source: We apply and evaluate our method on a mouse dataset, [47], provided by Mary Lyon Centre at MRC Harwell, Oxfordshire (MLC, Harwell). All the mice in the study are one-year old males of the C57BL/6Ntac strain. The mice are housed in groups of three (as a ‘cage’) and continuously recorded for a period of 3 to 4 days at a time, with a 12-hour lights-on, 12-hour lights-off cycle. The recordings are split into 30-minute periods, which form our unit of processing (segments). Since we are interested in their crepuscular rhythms, we selected the five segments straddling either side of the lights-on/off transitions at 07:00 and 19:00 every day. This gives us about 30 segments per cohort/cage: we had access to 16 distinct cohorts.

The data consists of single-channel IR side-view video (Fig. 1) and RFID position pickup in a coarse 3×6 antenna grid below the cage (Fig. 4 (b)), captured using one of four Home Cage Analyser (HCA) rigs Actual Analytics™: a prototypical setup is shown in Fig. 4 (a). Video is recorded at 25 frames per second (FPS), while the antenna baseplate is scanned at a rate of about 2Hz and upsampled to the frame rate. The latter, however, is noisy due to mouse huddling and climbing. The video also suffers from non-uniform lighting, occasional glare/blurring and clutter, particularly due to a movable tunnel and bedding. Most crucially, however, being single strain (and consequently of the same colour), and with no external markings, the mice are visually indistinguishable.

Pre-processing: We removed one of the cages as it had a non-standard setup. A calibration routine was then used to map all detections into the same frame of reference using a similarity transform. In order to maintain axis-aligned BBs, we transform the four corners of the BB but then define the transformed BB to be the one which intersects the midpoints of each transformed edge (we can do this because the rotation component is very minimal, $< 2^\circ$). A

minimal number of segments which exhibited anomalous readings (e.g. spurious/missing RFID traces) that could not be resolved were discarded altogether. (see Supplementary Material §A.1)

Ground-truthing: Using the VIA tool [48], we annotate video frames at four-second intervals for three-minute ‘snippets’ at the beginning, middle and end of each segment, as well as on the minute throughout the segment. This gives a good spread of samples with enough temporal continuity to evaluate our models. The annotations consist of an axis-aligned BB for each visible mouse, labelling the identity as Red/Green/Blue and the level of occlusion as clear vs. truncated: hidden mice are by definition not annotated. A *Difficult* flag is set when it is hard to make out the mouse even for a human observer. Where the identity of any mouse cannot be ascertained with certainty, this is noted in the schema and the frame discarded in the final evaluation. Refer to Supplementary Material §A.2 for further details.

Data splits: Our 15 cages (cohorts) were stratified into training (7), validation (3) and testing (5) (guaranteeing unbiased generalisation estimates). We annotated a random subset of 7 segments (3.5 Hrs) for training, 6 (3 Hrs) for validation and 10 (5 Hrs) for testing (2 per-cage). This yielded a total of 740 (training), 558 (validation) and 766 (testing) frames in which the mice could be unambiguously identified. We used all frames within the training/validation sets for optimising the weight model, but the rest of the architecture is trained and evaluated on three-minute snippets only, using 498, 398 and 699 frames respectively (for testing we remove snippets in which 50% or more of the frames show immobile mice or tentative/huddles due to severe occlusion.)

5.2 Comparison Methods

We compare the performance of our architecture to two simpler baseline models. The first, *Static (C)*, is a per-frame assignment (Hungarian algorithm) based on Euclidean distance between the centroid of the BBs and the projected RFID tag. The second model, *Static (P)*, uses the probabilistic weights of §3.3, but is assigned on a per-frame basis.

Our problem is quite unique for the reasons enumerated in §2, and hence, off-the-shelf solutions do not typically apply. For example, Bourached and Nachev [49] showed that the widely-used DeepLabCut [31] framework does not work on data from the Harwell lab, possibly because of the side-view causing extreme occlusion of key body parts. Other systems are either designed for singly-housed mice [50, 51] or leverage different fur-colours/external markings [24, 52] to identify the mice. We ran some experiments with *idtracker.ai* [30] but it yielded no usable tracks – the poor lighting of the cage, coupled with the side-view camera interfered with the background-subtraction method employed.

With regards to comparing with SOTA MOT trackers, we note that this is not meaningful – no matter the quality of the tracker, there is still the need for an identification stage, and hence, the comparison degenerates to optimising over tracker architectures (which is outside the scope of our research). However, by way of exploration, we can envision having a human-in-the-loop that seeds the track (if the tracker supports this) and provides the identifying information. To simulate this, we took each three-minute snippet, extracted the ground-truth annotation at the middle frame, and initialised a SiamMask [6] tracker per-mouse, which we ran forwards and backwards to either end of the snippet. We chose this tracker as it is designed to be a general purpose tracker with no need for pre-training on new data.

5.3 Evaluation

The standard MOT metrics (Multi-Object Tracking Precision (MOTP) and Multi-Object Tracking Accuracy (MOTA)) [53] do not sufficiently capture the needs of our problem, in that (a) we have a fixed set of objects we need to track (making the problem better defined), *but* (b) we also care about the absolute identity (i.e. permutations are not equivalent). While there is a similarity with object detection [54, 55] (using identity for object class), we know a priori that we cannot have more than one detection per ‘identity’ in each frame, and thus we modify existing metrics to suit our constraints.

Overall performance: We define the ‘Overall Accuracy’, A_O , as the ratio of ground-truths that are correctly identified: i.e. where the object is visible and the IoU between it and the identified BB is above a threshold, or when the object is hidden and the identifier outputs null.

For each (annotated) frame f and object j , we define a groundtruth BB, $GT_j^{(f)}$ — this is null when the object is hidden. The identifier itself outputs a single hypothesis $BB_j^{(f)}$ for object j , which can also be null. The Overall Accuracy, A_O is thus given by:

$$A_O(GT, BB) = \frac{1}{FJ} \sum_{f=1}^F \sum_{j=1}^J \Theta \left(BB_j^{(f)}, GT_j^{(f)} \right), \quad (7)$$

where

$$\Theta(B, G) \equiv \begin{cases} 1 & \text{if } B = \emptyset, G = \emptyset, \\ 1 & \text{if } IoU(B, G) > \phi, \\ 0 & \text{otherwise.} \end{cases} \quad (8)$$

We use an IoU threshold of 0.5 for normal objects, and 0.3 for annotations marked as *Difficult*.

A separate score, the ‘Overall IoU’, captures the average overlap between correct assignments, and is defined only for objects which are visible:

$$\Phi_O(GT, BB) = \frac{1}{\sum_F J^f} \sum_{f=1}^F \sum_{j=1}^{J^f} IoU(BB_j^{(f)}, GT_j^{(f)}), \quad (9)$$

where J^f includes only the visible animals in frame f . Note that we assume that the IoU between a ground-truth and a null identification is 0.

We also report the false negative rate (FNR) (visible objects that are not captured by a BB) and false positive rate (FPR) (hidden objects that are assigned a BB). The FPR is given by the average number of times a visible object is not assigned a BB by the identifier:

$$FPR_O = \frac{1}{\sum_F J^f} \sum_{f=1}^F \sum_{j=1}^{J^f} (BB_j^{(f)} = \emptyset \wedge GT_j^{(f)} \neq \emptyset), \quad (10)$$

where \wedge is the logical and. The FNR is the opposite metric counting the (average) number of times a hidden object is wrongly assigned a BB:

$$FNR_O = \frac{1}{\sum_F \bar{J}^f} \sum_{f=1}^F \sum_{j=1}^{\bar{J}^f} (BB_j^{(f)} \neq \emptyset \wedge GT_j^{(f)} = \emptyset), \quad (11)$$

where \bar{J}^f represents the set of animals hidden at frame f .

Performance conditioned on detections: The above metrics conflate the localisation of the BB (i.e. performance of the detector) with the identification error, which is what we actually seek to optimise. We thus define an additional metric conditioned on an oracle assignment of detections to ground-truth. Under the oracle, each candidate detection i is assigned to the ‘closest’ (by IoU) ground-truth annotation j using the Hungarian algorithm with a threshold of 0.5: this is relaxed to 0.3 for detections marked as *Difficult*. The identity of the detection $O_i^{(f)}$ is then that of the assigned ground-truth or, null if not assigned. Given the identity $ID_i^{(f)}$ assigned by our identifier to BB i , we define the Accuracy given Detections as the fraction of detections which are given the correct (same as oracle) assignment by the identifier (including null when required):

$$A_{GD} = \frac{1}{F} \sum_{f=1}^F \frac{1}{\bar{I}^{(f)}} \sum_{i=1}^{I^{(f)}} \delta(ID_i^{(f)}, O_i^{(f)}), \quad (12)$$

where $I^{(f)}$ is the number of detections in Frame f , and δ is the Kronecker delta (i.e. $\delta(i, j) = 1$ iff $i = j$ and 0 otherwise).

We also report the rate of mis-identifications (i.e. a wrong identity is assigned): these are BBs which are given an identity by the oracle and a different identity by the Identifier. For the purpose of this metric, null assignments are not counted as erroneous, and we normalise the count by the number of non-null oracle assignments.

Always relative to the oracle, we also quote the FPR and FNR. The FPR is now defined as the fraction of BBs with a null oracle assignment that are assigned an identity:

$$FPR_{GD} = \frac{\sum_{f=1}^F \sum_{i=1}^{I^{(f)}} (ID_i^{(f)} \neq \emptyset \wedge O_i^{(f)} = \emptyset)}{\sum_{f=1}^F \sum_{i=1}^{I^{(f)}} (O_i^{(f)} = \emptyset)}, \quad (13)$$

and conversely, the ratio of BBs with a non-null oracle assignment that are not identified define the FNR:

$$FNR_{GD} = \frac{\sum_{f=1}^F \sum_{i=1}^{I^{(f)}} (ID_i^{(f)} = \emptyset \wedge O_i^{(f)} \neq \emptyset)}{\sum_{f=1}^F \sum_{i=1}^{I^{(f)}} (O_i^{(f)} \neq \emptyset)}. \quad (14)$$

	Samples	Overall		Samples	Given detections	
		Visible	Hidden		Detections	Background
Train/Valid	2688	2541	147	2967	2235	732
Test	2097	2012	85	2504	1836	668

Table 1: Number of samples for evaluating the models according to the Overall and Given Detections metrics.

In fact, if we consider raw counts (rather than ratios), the sum of Mis-Identifications, FPR and FNR constitute all the errors the system makes.

Evaluation data-size: Table 1 summarises the number of samples (within each dataset) that are used to compute the above metrics. The Accuracy scores are normalised by the total number of samples in each case. The Overall IoU, mis-identification and FNR rates are divided by the Visible/Detections counts as necessary. FPR is always divided by the Hidden/Background counts.

5.4 Results

We comment on the quantitative performance of our approach. We also make available a sample of video-clips showing our framework in action at <https://github.com/michael-camilleri/TIM>: we comment on these in the Supplementary Material (see §D).

Performance on the test set: Table 2 shows the results of our model evaluated on the held-out test-set (the number of samples in each case appear in Table 1), where our scheme clearly outperforms all other methods on all metrics. Table 3 on the other hand shows the raw counts of the same metrics as Table 2. The overall accuracy is quite high, 77%, especially given the maximum possible recall of the FCOS detector of 0.90 (§4) which is in effect an upper bound. The FPR seems high, but in reality, the number of hidden samples is only 85 (4%) when looking at Table 3 — indeed, false negatives are a much bigger factor overall.

Model	Overall				Given Detections			
	$A_O \uparrow$	IoU \uparrow	FNR \downarrow	FPR \downarrow	$A_{GD} \uparrow$	Mis-ID \downarrow	FNR \downarrow	FPR \downarrow
Static (C)	0.659	0.626	0.322	0.788	0.623	0.178	0.122	0.590
Static (P)	0.716	0.666	0.264	0.741	0.694	0.138	0.100	0.496
Ours	0.767	0.694	0.215	0.659	0.791	0.104	0.066	0.317

Table 2: Comparative Results on the Test-Set for the Overall Accuracy, and Accuracy Given Detections. *Static (C)* is a baseline, *Static (P)* uses our weight model on a per-frame basis and the full temporal identifier is labelled *Ours*.

The contrast between methods is starker when it comes to the analysis given detections: this is because in the former, the performance of the detector acts as an equaliser between alternatives, but A_{GD} teases out the capability of the identification system separately from the quality of the detector. Here the FPR is lower, although from the point of view of detections, there are more of them that should be null (668 or 27%). Note that the number of background BBs, (impacting the FPR) is higher. We also investigated outlier models which were fit explicitly to the outliers in our data but validation-set evaluation yielded a drop in performance.

Model	Overall			Given Detections			
	$A_O \uparrow$	FNR \downarrow	FPR \downarrow	$A_{GD} \uparrow$	Mis-ID \downarrow	FNR \downarrow	FPR \downarrow
Static (C)	1382	648	67	1559	327	224	394
Static (P)	1502	532	63	1737	253	183	331
Ours	1608	433	56	1980	191	121	212
Normaliser	2097	2012	85	2504	2504	1836	668

Table 3: Counts of Performance metrics on the Test-Set (counterpart to Table 1). IoU has no meaning as a count. The last row shows the normaliser which would be used in computing rates.

	$A_O \uparrow$	IoU \uparrow	FNR \downarrow	FPR \downarrow
SiamMask (Rate)	0.637	0.565	0.336	1.000
SiamMask (Count)	1335	—	677	85
Normaliser	2097	2097	2012	85

Table 4: Overall Performance of the SiamMask tracker on the Test-Set. The normaliser is replicated here from Table 3 for completeness.

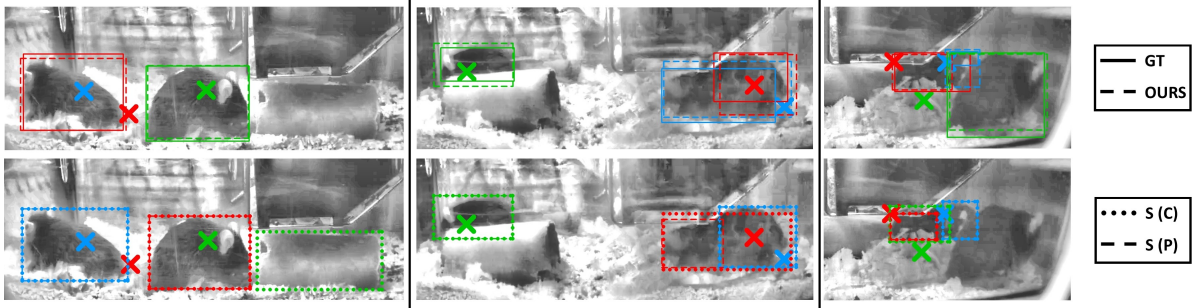


Figure 5: Examples of successful identifications (cropped to appropriate regions and brightened with CLAHE for clarity). The ground-truth and identifications according to our model appear in the top row, while the bottom row shows the identifications due to the other two methods.

Alternative solutions: We also present the performance of the SiamMask [6] tracker in Table 4. We can only report the Overall performance metrics, since SiamMask does not use our detections. Despite this having access to the ground-truth data for initialisation, it only achieved 0.637 Overall Accuracy on our test-set, less than the baseline method. The clear shortcoming of this method is that it cannot handle occlusion and hidden objects: note how the FPR is 1, because it will always attempt to find a BB for each mouse. Notwithstanding this, the IoU and FNR are also quite poor and worse than our baseline. One has to keep in mind that this method had no pre-training on our data, and in this respect, its performance is quite impressive, given that the statistics of our videos are somewhat different from typical videos on the web, and certainly more challenging. At the same time, we should point out that while one could argue that this puts it at a disadvantage compared to our detector which was fine-tuned on our data, the tracker itself is initialised from ground-truth detections and hence has access to more information than our identifier.

Example Identifications: Fig. 5 shows some sample visualisations of the identification using our method (top) and the baseline/ablation models (bottom). Note how in the leftmost frame, our method is able to disregard the spurious tunnel detection as well as use temporal context to reason about the occlusion of the Blue mouse by the Red one — the probabilistic weighting alone is unable to account for this, although it does reject the tunnel to the outlier model. The same happens in the centre frame between Red/Blue: indeed, the static probabilistic weighting is in error on the extent of what should be the Blue mouse in addition to mis-identifying it. The rightmost frame is particularly challenging due to the close proximity of all mice, and yet, our method makes them out well (the almost fully occluded Blue mouse is considered a *Difficult* detection).

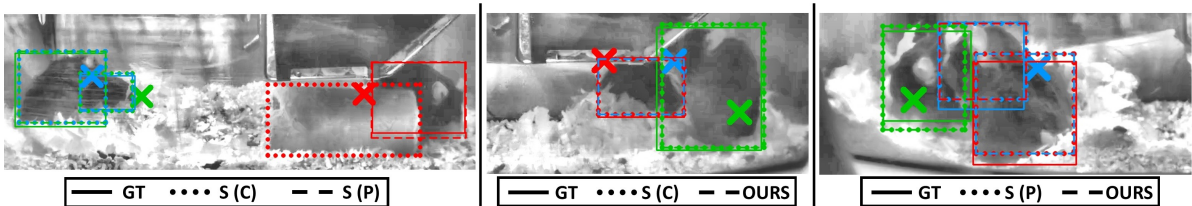


Figure 6: Analysis of sub-optimal identifications. The ground-truth is shown as a solid BB with different methods appearing as dashed/dotted lines (legend below each frame).

In Fig. 6, we study some more difficult cases. The leftmost frame shows the impact of the probabilistic weighting (Static (P)) as opposed to the centroid-distance (Static (C)). Note how due to the Gaussian model on BB centroid and size, it is able to correctly pick out the Red mouse. This is also what allows it to reason about the occluded Blue

mouse huddling with Green, despite the RFID seemingly showing the contrary. On the other hand, the same model does sometimes hurt performance: in the centre frame, it classifies Red as Blue, although this is a particularly difficult frame and in annotation, the correct identity was only made out after many passes and stepping through frames. Similarly, sometimes it is the temporal aspect which hurts performance, due to tracklets switching identities mid-way (which is not catered for by our ILP), as happens between Red/Blue in the rightmost frame.

6 Conclusions

We have proposed an ILP formulation for identifying visually similar animals in a crowded cage using weak localisation information. Using our novel probabilistic model of object detections, coupled with the tracker-based combinatorial identification, we are able to correctly identify the mice 77% of the time, even under very challenging conditions. Our approach is also applicable to other scenarios which require fusing external sources of identification to video data. We are currently looking towards extending the weight model to take into account the orientation of the animals as this allows us to reason about the relative position of the BB to the RFID pickup, as well as modelling the tunnel which can occlude the mice.

Acknowledgements

We thank our collaborators at the Mary Lyon Centre at MRC Harwell, Oxfordshire, especially Dr Sara Wells and Dr Pat Nolan for providing and explaining the data set. MC's work was supported by the EPSRC Centre for Doctoral Training in Data Science, funded by the UK Engineering and Physical Sciences Research Council (grant EP/L016427/1) and the University of Edinburgh. LZ was supported by NSFC (No. 6210020439). RSB was supported by funding to MLC, Harwell from the Medical Research Council UK (grant A410). Funding was also provided by the EPSRC Programme Grant Seebibyte EP/M013774/1.

Ethical approval

Data collection for all animal studies and procedures used in the mouse dataset were carried out at MLC, Harwell, in accordance with the Animals (Scientific Procedures) Act 1986, UK, Amendment Regulations 2012 (SI 4 2012/3039) as indicated in [47].

References

- [1] J. Silva, N. Lau, J. Rodrigues, J. L. Azevedo, and A. J. R. Neves, "Sensor and Information Fusion Applied to a Robotic Soccer Team," in *RoboCup 2009: Robot Soccer World Cup XIII*, J. Baltus, M. G. Lagoudakis, T. Naruse, and S. S. Ghidary, Eds. Berlin, Heidelberg: Springer Berlin Heidelberg, 2010, pp. 366–377.
- [2] A. Bewley, Z. Ge, L. Ott, F. Ramos, and B. Upcroft, "Simple online and realtime tracking," in *Proceedings - International Conference on Image Processing, ICIP*, vol. 2016-Augus. IEEE Computer Society, aug 2016, pp. 3464–3468.
- [3] S. D. M. Brown and M. W. Moore, "Towards an encyclopaedia of mammalian gene function: the International Mouse Phenotyping Consortium," *Disease Models & Mechanisms*, vol. 5, no. 3, pp. 289–292, may 2012. [Online]. Available: <http://www.ncbi.nlm.nih.gov/pubmed/22566555>
- [4] K. Zuiderveld, "Contrast limited adaptive histogram equalization," in *Graphics gems*, P. S. Heckbert, Ed. Academic Press, 1994, pp. 474 – 485.
- [5] L. Leal-Taixé, A. Milan, K. Schindler, D. Cremers, I. Reid, and S. Roth, "Tracking the Trackers: An Analysis of the State of the Art in Multiple Object Tracking," *arXiv preprint*, vol. cs.CV, apr 2017. [Online]. Available: <http://arxiv.org/abs/1704.02781>
- [6] Q. Wang, L. Zhang, L. Bertinetto, W. Hu, and P. H. S. Torr, "Fast online object tracking and segmentation: A unifying approach," in *Proceedings of the IEEE Conference on Computer Vision and Pattern Recognition*, 2019, pp. 1328–1338.
- [7] Y. Zhang, C. Wang, X. Wang, W. Zeng, and W. Liu, "FairMOT: On the Fairness of Detection and Re-Identification in Multiple Object Tracking," *arXiv preprint*, vol. cs.CV, apr 2020. [Online]. Available: <http://arxiv.org/abs/2004.01888>

- [8] J. Peng, C. Wang, F. Wan, Y. Wu, Y. Wang, Y. Tai, C. Wang, J. Li, F. Huang, and Y. Fu, “Chained-Tracker: Chaining Paired Attentive Regression Results for End-to-End Joint Multiple-Object Detection and Tracking,” in *Lecture Notes in Computer Science (including subseries Lecture Notes in Artificial Intelligence and Lecture Notes in Bioinformatics)*, vol. 12349. Glasgow: Springer Science and Business Media Deutschland GmbH, aug 2020, pp. 145–161. [Online]. Available: https://link.springer.com/chapter/10.1007/978-3-030-58548-8_{_}9
- [9] L. Leal-Taixé, A. Milan, I. Reid, S. Roth, and K. Schindler, “MOTChallenge 2015: Towards a Benchmark for Multi-Target Tracking,” *arXiv preprint*, vol. cs.CV, apr 2015. [Online]. Available: <http://arxiv.org/abs/1504.01942>
- [10] P. Dendorfer, H. Rezatofighi, A. Milan, J. Shi, D. Cremers, I. Reid, S. Roth, K. Schindler, and L. Leal-Taixé, “MOT20: A benchmark for multi object tracking in crowded scenes,” *arXiv*, vol. cs.CV, no. 2003.09003, mar 2020. [Online]. Available: <http://arxiv.org/abs/2003.09003>
- [11] A. Dave, T. Khurana, P. Tokmakov, C. Schmid, and D. Ramanan, “TAO: A Large-Scale Benchmark for Tracking Any Object,” in *Computer Vision – ECCV 2020*, A. Vedaldi, H. Bischof, T. Brox, and J.-M. Frahm, Eds. Cham: Springer International Publishing, 2020, pp. 436–454.
- [12] L. Lan, X. Wang, G. Hua, T. S. Huang, and D. Tao, “Semi-online Multi-people Tracking by Re-identification,” *International Journal of Computer Vision*, vol. 128, no. 7, pp. 1937–1955, jul 2020. [Online]. Available: <https://doi.org/10.1007/s11263-020-01314-1>
- [13] S. Tang, M. Andriluka, B. Andres, and B. Schiele, “Multiple People Tracking by Lifted Multicut and Person Re-identification,” in *2017 IEEE Conference on Computer Vision and Pattern Recognition (CVPR)*. Honolulu, Hawaii: IEEE, jul 2017, pp. 3701 – 3710. [Online]. Available: <http://ieeexplore.ieee.org/document/8099877/>
- [14] L. Bergamini, S. Pini, A. Simoni, R. Vezzani, S. Calderara, R. D’Eath., and R. Fisher, “Extracting Accurate Long-Term Behavior Changes from a Large Pig Dataset,” in *Proceedings of the 16th International Joint Conference on Computer Vision, Imaging and Computer Graphics Theory and Applications - Volume 5: VISAPP*, University of Edinburgh. SciTePress, 2021, pp. 524–533.
- [15] S.-I. Yu, Y. Yang, X. Li, and A. G. Hauptmann, “Long-Term Identity-Aware Multi-Person Tracking for Surveillance Video Summarization,” *arXiv*, vol. cs.CV, no. 1604.07468, apr 2016. [Online]. Available: <http://arxiv.org/abs/1604.07468>
- [16] L. Fagot-Bouquet, R. Audigier, Y. Dhome, and F. Lerasle, “Improving Multi-frame Data Association with Sparse Representations for Robust Near-online Multi-object Tracking,” in *Computer Vision – ECCV 2016*, B. Leibe, J. Matas, N. Sebe, and M. Welling, Eds. Cham: Springer International Publishing, 2016, pp. 774–790.
- [17] S. Tang, M. Andriluka, and B. Schiele, “Detection and Tracking of Occluded People,” *International Journal of Computer Vision*, vol. 110, no. 1, pp. 58–69, oct 2014. [Online]. Available: <https://doi.org/10.1007/s11263-013-0664-6>
- [18] F. Fleuret, H. Ben Shitrit, and P. Fua, “Re-Identification for Improved People Tracking,” *Person Re-Identification*, pp. 309–330, 2014. [Online]. Available: <http://infoscience.epfl.ch/record/192416>
- [19] M. Ye, J. Shen, G. Lin, T. Xiang, L. Shao, and S. C. Hoi, “Deep Learning for Person Re-identification: A Survey and Outlook,” *IEEE Transactions on Pattern Analysis and Machine Intelligence*, no. 01, pp. 1–1, 2021. [Online]. Available: <https://ieeexplore.ieee.org/document/9336268/>
- [20] M. Qiao, T. Zhang, C. Segalin, S. Sam, P. Perona, and M. Meister, “Mouse Academy: high-throughput automated training and trial-by-trial behavioral analysis during learning,” *bioRxiv*, pp. 1 — 50, nov 2018. [Online]. Available: <https://www.biorxiv.org/content/10.1101/467878v1>
- [21] A. B. Wiltschko, M. J. Johnson, G. Iurilli, R. E. Peterson, J. M. Katon, S. L. Pashkovski, V. E. Abraira, R. P. Adams, and S. R. Datta, “Mapping Sub-Second Structure in Mouse Behavior.” *Neuron*, vol. 88, no. 6, pp. 1121–1135, dec 2015. [Online]. Available: <http://www.ncbi.nlm.nih.gov/pubmed/26687221>
- [22] M. Tufail, F. Coenen, T. Mu, and S. J. Rind, “Mining Movement Patterns from Video Data to Inform Multi-agent Based Simulation,” in *Agents and Data Mining Interaction*, L. Cao, Y. Zeng, B. An, A. L. Symeonidis, V. Gorodetsky, F. Coenen, and P. S. Yu, Eds. Cham: Springer International Publishing, 2015, pp. 38–51.
- [23] B. Q. Geuther, S. P. Deats, K. J. Fox, S. A. Murray, R. E. Braun, J. K. White, E. J. Chesler, C. M. Lutz, and V. Kumar, “Robust mouse tracking in complex environments using neural networks,” *Communications Biology*, vol. 2, no. 1, pp. 1–11, dec 2019. [Online]. Available: <https://www.nature.com/articles/s42003-019-0362-1>
- [24] C. Segalin, J. Williams, T. Karigo, M. Hui, M. Zelikowsky, J. Sun, P. Perona, D. J. Anderson, and A. Kennedy, “The Mouse Action Recognition System (MARS): a software pipeline for automated analysis of social behaviors in mice,” *bioRxiv*, jul 2020. [Online]. Available: <https://doi.org/10.1101/2020.07.26.222299>

- [25] F. de Chaumont, E. Ey, N. Torquet, T. Lagache, S. Dallongeville, A. Imbert, T. Legou, A.-M. L. Sourd, P. Faure, T. Bourgeron, and J.-C. Olivo-Marin, “Live Mouse Tracker: real-time behavioral analysis of groups of mice,” *bioRxiv*, 2018. [Online]. Available: <https://www.biorxiv.org/content/early/2018/06/18/345132>
- [26] Z. Jiang, Z. Liu, L. Chen, L. Tong, X. Zhang, X. Lan, D. Crookes, M.-H. Yang, and H. Zhou, “Detection and Tracking of Multiple Mice Using Part Proposal Networks,” *arXiv preprint*, vol. cs.CV, no. 1906.02831, jun 2019. [Online]. Available: <http://arxiv.org/abs/1906.02831>
- [27] A. Sadafi, V.-M. Katsageorgiou, H. Huang, F. Papaleo, V. Murino, and D. Sona, “Multiple Mice Tracking: Occlusions Disentanglement using a Gaussian Mixture Model,” in *2018 24th International Conference on Pattern Recognition (ICPR)*. Beijing, China: IEEE, aug 2018, pp. 2433–2437. [Online]. Available: <https://ieeexplore.ieee.org/document/8545402/>
- [28] L. Giancardo, D. Sona, H. Huang, S. Sannino, F. Managò, D. Scheggia, F. Papaleo, and V. Murino, “Automatic Visual Tracking and Social Behaviour Analysis with Multiple Mice,” *PLOS ONE*, vol. 8, no. 9, pp. 1 — 14, 2013. [Online]. Available: <https://doi.org/10.1371/journal.pone.0074557>
- [29] M. Lorbach, R. Poppe, and R. C. Veltkamp, “Interactive rodent behavior annotation in video using active learning,” *Multimedia Tools and Applications*, feb 2019. [Online]. Available: <https://doi.org/10.1007/s11042-019-7169-4>
- [30] F. Romero-Ferrero, M. G. Bergomi, R. C. Hinz, F. J. Heras, and G. G. de Polavieja, “idtracker.ai: tracking all individuals in small or large collectives of unmarked animals,” *Nature Methods*, vol. 16, no. 2, pp. 179–182, feb 2019. [Online]. Available: <https://doi.org/10.1038/s41592-018-0295-5>
- [31] A. Mathis, P. Mamidanna, K. M. Cury, T. Abe, V. N. Murthy, M. W. Mathis, and M. Bethge, “DeepLabCut: markerless pose estimation of user-defined body parts with deep learning,” *Nature Neuroscience*, vol. 21, no. September, pp. 1281 – 1289, 2018. [Online]. Available: <https://doi.org/10.1038/s41593-018-0209-y>
- [32] A. Hoffman and J. Kruskal, “Integral Boundary Points of Convex Polyhedra,” in *50 Years of Integer Programming 1958-2008: From the Early Years to the State-of-the-Art*, M. Junger, T. Liebling, D. Naddef, G. Nemhauser, W. Pulleyblank, G. Reinelt, G. Rinaldi, and L. Wolsey, Eds. Springer-Verlag, 2010, vol. 38, ch. 3, pp. 49–76.
- [33] V. V. Vazirani, *Approximation Algorithms*. Springer Berlin Heidelberg, 2003.
- [34] R. M. Karp, “Reducibility among Combinatorial Problems,” in *Complexity of Computer Computations: Proceedings of a symposium on the Complexity of Computer Computations, held March 20–22, 1972, at the IBM Thomas J. Watson Research Center, Yorktown Heights, New York, and sponsored by the Office of Naval Research, Ma*, R. E. Miller, J. W. Thatcher, and J. D. Bohlinger, Eds. Boston, MA: Springer US, 1972, pp. 85–103. [Online]. Available: <https://doi.org/10.1007/978-1-4684-2001-2{-}9>
- [35] Q. S. Hua, Y. Wang, D. Yu, and F. C. Lau, “Dynamic programming based algorithms for set multicover and multiset multicover problems,” *Theoretical Computer Science*, vol. 411, no. 26-28, pp. 2467–2474, jun 2010.
- [36] Y. Bar-Shalom, F. Daum, and J. Huang, “The Probabilistic Data Association Filter: Estimation in the presence of measurement origin uncertainty,” *IEEE Control Systems*, vol. 29, no. 6, pp. 82–100, 2009.
- [37] H. Jiang, S. Fels, and J. J. Little, “A linear programming approach for multiple object tracking,” *Proceedings of the IEEE Computer Society Conference on Computer Vision and Pattern Recognition*, 2007.
- [38] X. Wang, E. Türetken, F. Fleuret, and P. Fua, “Tracking Interacting Objects Optimally Using Integer Programming,” *Lecture Notes in Computer Science (including subseries Lecture Notes in Artificial Intelligence and Lecture Notes in Bioinformatics)*, vol. 8689 LNCS, no. PART 1, pp. 17–32, 2014. [Online]. Available: <https://link.springer.com/chapter/10.1007/978-3-319-10590-1{-}2>
- [39] S. H. Rezatofighi, A. Milan, Z. Zhang, Q. Shi, A. Dick, and I. Reid, “Joint Probabilistic Data Association Revisited,” in *2015 IEEE International Conference on Computer Vision (ICCV)*, dec 2015, pp. 3047–3055.
- [40] Z. Tian, C. Shen, H. Chen, and T. He, “FCOS: Fully Convolutional One-Stage Object Detection,” in *2019 IEEE/CVF International Conference on Computer Vision (ICCV)*, 2019, pp. 9626–9635.
- [41] K. He, X. Zhang, S. Ren, and J. Sun, “Deep Residual Learning for Image Recognition,” in *2016 IEEE Conference on Computer Vision and Pattern Recognition (CVPR)*, jun 2016, pp. 770–778.
- [42] C. Kim, F. Li, A. Ciptadi, and J. M. Rehg, “Multiple Hypothesis Tracking Revisited,” in *2015 IEEE International Conference on Computer Vision (ICCV)*, dec 2015, pp. 4696–4704.
- [43] G. Bhat, M. Danelljan, L. Van Gool, and R. Timofte, “Know Your Surroundings: Exploiting Scene Information for Object Tracking,” in *Computer Vision – ECCV 2020*, A. Vedaldi, H. Bischof, T. Brox, and J.-M. Frahm, Eds. Glasgow: Springer International Publishing, 2020, pp. 205–221.
- [44] T. A. M. Toffolo and H. G. Santos, “Python-MIP.” [Online]. Available: <https://python-mip.com/>

- [45] J. Forrest and R. Lougee-Heimer, “CBC User’s Guide.” [Online]. Available: <https://coin-or.github.io/Cbc/>
- [46] J. Forrest, D. de la Nuez, and R. Lougee-Heimer, “CLP User Guide.” [Online]. Available: <https://www.coin-or.org/Clp/userguide/index.html>
- [47] R. S. Bains, H. L. Cater, R. R. Sillito, A. Chartsias, D. Sneddon, D. Concas, P. Keskivali-Bond, T. C. Lukins, S. Wells, A. Acevedo Arozena, P. M. Nolan, and J. D. Armstrong, “Analysis of Individual Mouse Activity in Group Housed Animals of Different Inbred Strains using a Novel Automated Home Analysis System,” *Frontiers in Behavioral Neuroscience*, vol. 10, p. 106, jun 2016.
- [48] A. Dutta and A. Zisserman, “The VIA Annotation Software for Images, Audio and Video,” in *Proceedings of the 27th ACM International Conference on Multimedia*, ser. MM ’19. New York, NY, USA: ACM, 2019. [Online]. Available: <https://doi.org/10.1145/3343031.3350535>
- [49] A. Bourached and P. Nachev, “Unsupervised Videographic Analysis of Rodent Behaviour,” *arXiv*, vol. cs.Cv, no. 1910.11065, oct 2019. [Online]. Available: <http://arxiv.org/abs/1910.11065>
- [50] J. M. Graving, D. Chae, H. Naik, L. Li, B. Koger, B. R. Costelloe, and I. D. Couzin, “DeepPoseKit, a software toolkit for fast and robust animal pose estimation using deep learning,” *eLife*, vol. 8, oct 2019.
- [51] T. D. Pereira, D. E. Aldarondo, L. Willmore, M. Kislin, S. S. Wang, M. Murthy, and J. W. Shaevitz, “Fast animal pose estimation using deep neural networks,” *Nature Methods*, vol. 16, no. 1, pp. 117–125, jan 2019. [Online]. Available: <https://doi.org/10.1038/s41592-018-0234-5>
- [52] M. Souriou, E. Bestaven, E. Guillaud, S. Bertrand, M. Cabanas, L. Milan, W. Mayo, M. Garret, and J.-R. Cazalets, “3-D motion capture for long-term tracking of spontaneous locomotor behaviors and circadian sleep/wake rhythms in mouse,” *Journal of Neuroscience Methods*, vol. 295, pp. 51–57, feb 2018. [Online]. Available: <https://www.sciencedirect.com/science/article/pii/S0165027017304041>
- [53] K. Bernardin and R. Stiefelagen, “Evaluating Multiple Object Tracking Performance: The CLEAR MOT Metrics,” *EURASIP Journal on Image and Video Processing*, vol. 2008, no. 1, may 2008. [Online]. Available: <https://doi.org/10.1155/2008/246309>
- [54] M. Everingham, S. M. Eslami, L. Van Gool, C. K. Williams, J. Winn, and A. Zisserman, “The PASCAL Visual Object Classes Challenge: A Retrospective,” *International Journal of Computer Vision*, vol. 111, no. 1, pp. 98–136, jun 2014. [Online]. Available: <https://link.springer.com/article/10.1007/s11263-014-0733-5>
- [55] T.-Y. Lin, M. Maire, S. Belongie, J. Hays, P. Perona, D. Ramanan, P. Dollár, and C. L. Zitnick, “Microsoft COCO: Common Objects in Context,” in *Computer Vision – ECCV 2014*, D. Fleet, T. Pajdla, B. Schiele, and T. Tuytelaars, Eds. Cham: Springer International Publishing, 2014, pp. 740–755.

TRACKING AND LONG-TERM IDENTIFICATION USING NON-VISUAL MARKERS

SUPPLEMENTARY MATERIAL

A Dataset

In this section we elaborate on the Dataset used in our work, including the annotation schema used. Please refer to our online repository at <https://github.com/michael-camilleri/TIM> for an example clip of our data.

A.1 Data cleaning and calibration

We removed one of the cages as it had a non-standard setup. The Radio-Frequency Identification (RFID) metadata was then filtered through consistency logic to ensure that the same mice were visible in all recordings from the same cage and that there was no missing data. In some cases, missing data due to huddling mice (which causes the RFID to be jumbled) could be filled in by looking at neighbouring periods to see if the mice moved in between and if not the same position filled in: otherwise, the segment was discarded. Segments in which there was a significant timing mismatch between recording time and RFID traces (indicating a possible invalid trace) were also discarded.

Since the data was captured using one of four different rigs, a calibration routine was required to bring all videos in the same frame of reference, simplifying downstream processing. We were given access to a number of calibration videos for each rig at multiple points throughout the data collection process (but always in between whole recordings), yielding 8 distinct configurations. Using a checkerboard pattern on the bottom of the rig (see Fig. 4(b) in main paper), we annotated 18 reproducible points, which we split into training (odd) and validation (even) sets. Note that the chosen points correspond to the centres of the RFID antennas on the baseplate, but this is immaterial to this calibration routine. We then used the training set of points to fit affine transforms of varying complexity and also optimised which setup to use as the prototype. We found that a Similarity transform proved ideal in terms of residuals on the validation set, as seen in Fig. A.1.

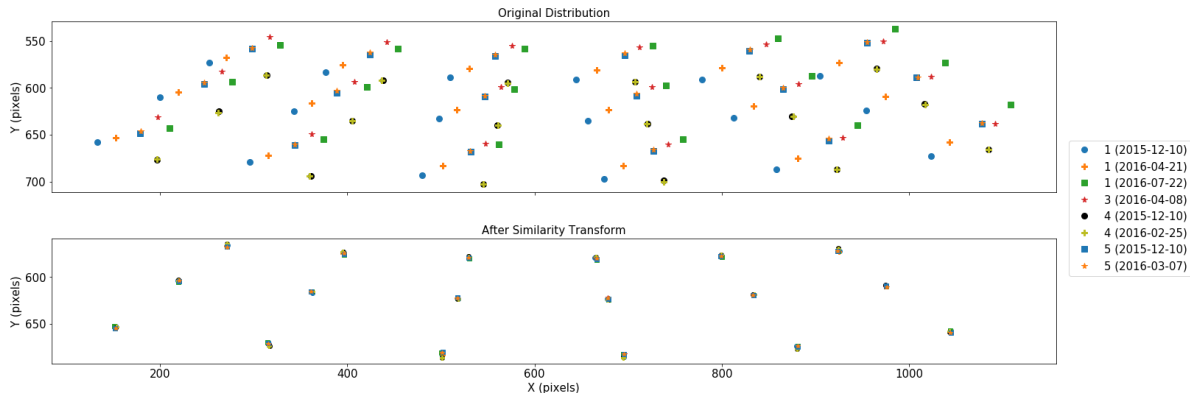


Figure A.1: Distribution of Calibration points across setups, before (top) and after (bottom) calibration.

A.2 Annotation schema

We annotated our data using the VIA tool [1]. The annotation requires drawing axis-aligned Bounding Boxes (BBs) around the mice and the tunnel: the latter was included since we expect future work to incorporate the presence of the tunnel in reasoning about occlusion. For each frame, we annotate all visible objects (mice/tunnel): hidden objects are defined by their missing an annotation. For the mice we do not include the tail or the paws in the BB: the tunnel includes the opening. For each annotation, we specify:

- The identity of the mouse as Red/Green/Blue: we allow specifying multiple tentative identities when it cannot be ascertained with certainty, or when the mice are huddling and immobile (in the latter case, the BB extends over the huddle).
- The level of occlusion: Clear, Truncated or NA when it is difficult to judge/marginal. Note that for this purpose, truncation refers to the size of the BB relative to how it would like like if the mouse were not occluded. In other words, it may be possible for a mouse to be partially occluded in such a way that the BB is not Truncated.
- For detections which are hard to make out even for a human annotator, e.g. when the mouse is almost fully occluded, a ‘Difficult’ flag is set.

Our policy was to annotate frames at 4s intervals. Within each 30-minute segment, we annotate three snippets, at 00:00 – 03:00, 13:32 – 16:28 and 27:00 – 29:56. The last snippet does not include 30:00, since the last recorded frame is just before the 30:00 minute mark. In some segments, we alternatively/also annotate every minute on the minute, again with the caveat that the last annotation is at 29:56 to follow the 4s rule.

B Theory

B.1 ILP formulation as covering problem

We show that our Integer Linear Programming (ILP) formulation is a special case of the covering problem.

A covering problem can be expressed as a linear program as follows:

$$\text{minimise } \sum_e c_e x_e, \quad (\text{B.1})$$

$$\text{subject to } \sum_f d_{fe} x_f \geq 1 \forall e \quad (\text{B.2})$$

$$x_e \in \{0, 1\} \quad (\text{B.3})$$

in which, the constraint coefficients d and the objective costs c are *non-negative* [2, p. 109]. Note that to avoid confusion, we represent the constraints by d (rather than a which we use for the assignment in the main body of our paper).

Let

$$\mathbf{x} \equiv [\mathbf{a}_0^\top, \dots, \mathbf{a}_{I+T}^\top]^\top, \quad (\text{B.4})$$

represent the flattened assignment matrix A , where \mathbf{a}_i are the rows of the original matrix. Index e is consequently the index over i/j in row-major order given by:

$$e = (i - 1)(J + 1) + j \quad \forall i \in I + T, j \in J + 1. \quad (\text{B.5})$$

If we assume that log-probabilities are always negative, our original objective, Eq. (1) involves *maximising* a sum of *negative* weights, which is equivalent to minimising the sum of the negated weights, and thus would fit the condition that the c_e ’s in Eq. (B.1) should be non-negative. In reality, probability densities may be greater than 1, and hence our assumption that the weight is always negative may not hold. However, we can circumvent this if we note that after computing all the weights, we can subtract a constant term such that all weights are negative. This means we can define c as:

$$\mathbf{c} \equiv [-\mathbf{w}_0^\top + k\mathbf{1}, \dots, -\mathbf{w}_{I+T}^\top + k\mathbf{1}]^\top, \quad (\text{B.6})$$

where \mathbf{w}_i are again the rows of the original weight matrix. In this case, k would be the maximum value over W , added to all the elements, such that $\min c = 0$. Note that in our implementation we do not need to do this, since the solver is not impacted by the formulation as a covering problem.

As for the constraints of our original formulation, Eqs. (2–4), these are all summations over the assignment matrix (now represented by x), and the coefficients $d_{fe} \in \{0, 1\}$ are clearly non-negative as required in the covering problem formulation.

B.2 Motivation for Performance given detections

Consider the scenario in Fig. B.1. The ground-truth assignment for the ‘Blue’ mouse is shown as a blue BB: however, the detector only outputs the BB in magenta. Clearly, the right thing for the identifier to do is to not assign the magenta BB to any mouse, especially if the system is to be used down the line to say predict mouse behaviour. However, under the definition of overall accuracy, whatever the identifier does, its score on this sample will always be 0.

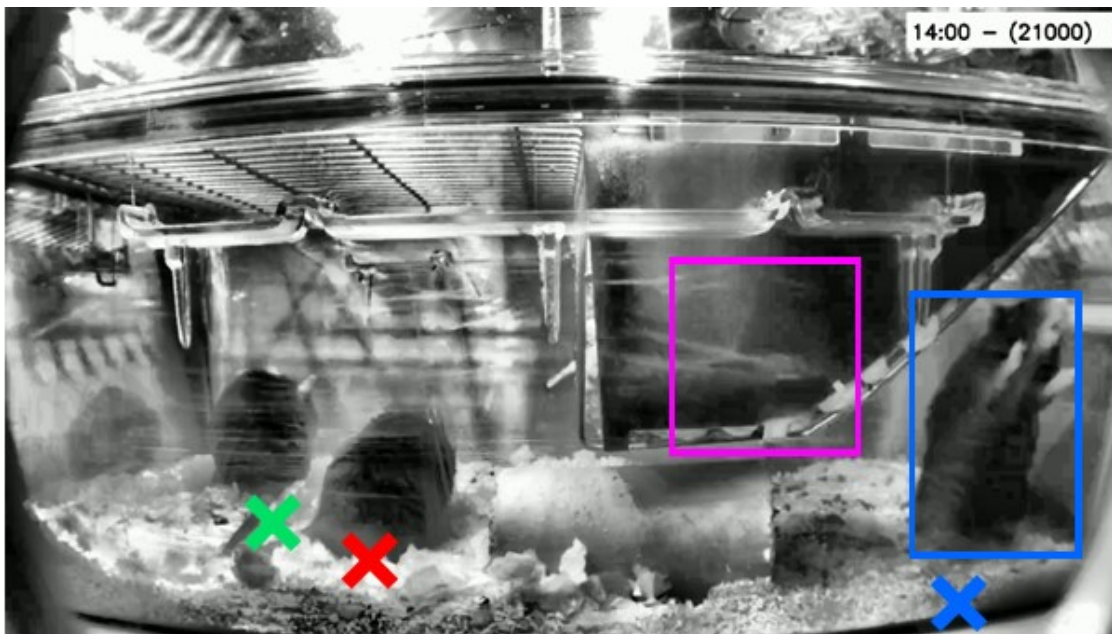


Figure B.1: Hypothetical scenario in which the performance of the Identifier is overshadowed by the detector (only Blue ground-truth is shown to reduce clutter).

Our metrics conditioned on the oracle assignment are designed to handle such cases, and tease out the performance of the Identifier from any shortcomings of the detector. Note how in the same example, the oracle assignment will reject the magenta BB as having no identity: hence, the identifier can now get a perfect score if it correctly rejects the BB. This is possible because of the key difference between A_O and A_{GD} : the former evaluates how well objects j are identified, but the latter measures identification performance for detections i .

C Fine-Tuning

In this section, we comment on the various details of the methods employed, including how we came to chose certain configurations over others.

C.1 Finetuning the Detector

We use the network pre-trained on CoCo [3] with the typical “1x” training settings (see public codebase¹). We remove the *COCO* classifier layer of 81 classes and set a randomly initialised classifier with three categories (i.e., *mouse*, *tunnel* and *background*), and proceed to optimise the weights of the entire network. We investigate training using either: (a) the full set of 3247 annotated frames (BBs without identities), or (b) a reduced subset of 3152 frames, discarding frames marked as Difficult (see §A.2). We set a constant learning rate 0.0001 for 30,000 iterations with batch size 16, checkpointing every 1000 iterations. Evaluation on the held-out annotations from the validation set, indicated that the best performing model was that trained on the reduced subset (b), for 11,000 iterations.

C.2 Finetuning Tracker parameters

Using the combined training/validation set, we ran the identification process using our ILP method for different combinations of the parameters, in a grid-search, with Intersection-over-Union (IoU) $\in \{0.65, 0.7, 0.75, 0.8, 0.85, 0.9\}$

¹<https://github.com/tianzhi0549/FCOS>

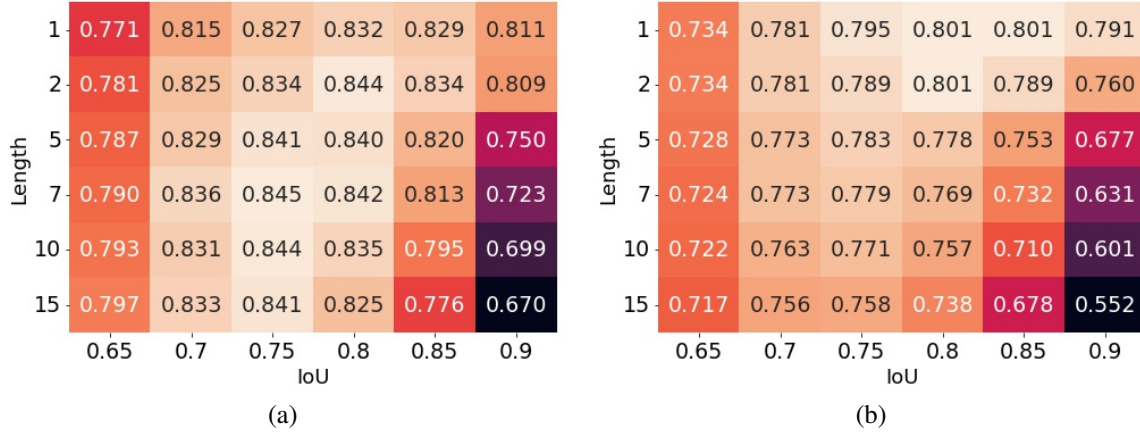


Figure C.1: Accuracy (a) given detections, and (b) overall, for various configurations of the tracker IoU threshold and the minimum tracklet length.

and length $\in \{1, 2, 5, 7, 10, 15\}$. The resulting accuracies appear in Fig. C.1. In terms of the metric given detections, (a), the best score is achieved with $L = 7$ and IoU= 0.75. However, we see that the alternative configuration $L = 2$, IoU= 0.8 is only marginally worse, and it is also among the optimal in terms of Overall Accuracy (b). We thus opted for the latter configuration as a compromise between the two scores.

C.3 Finetuning the Weight model

Tuning the parameters of the weight model is perhaps the central aspect which governs the performance of our solution. We document this in some depth below.

Choice of Context Vector: Using data from the combined training/validation set, and ignoring marginal visibility outcomes, we compared the mutual information between various choices of summarising the configuration c and the annotated visibility, and settled on counting the number of occupancies in each cell as the imparting the most information. This is natural, but we wanted to see if there was any simpler representation (such as leveraging left/right symmetry).

Predicting v_j : Given position p_j and context c_j , our next task is to generate a distribution over visibility v_j . We explored using multinomial Linear Regression (LR), Naïve Bayes (NB), decision trees, Random Forests (RFs) and three-layer Neural Networks (NNs), all of which we optimised using 5-fold cross-validation on the combined training/validation data. Note that since we will be summing out v_j , getting a calibrated distribution is the key requirement, and hence, when choosing/optimising the models, we used the held-out data log-likelihood as our objective. Our best score was achieved with a RF classifier, with 100 estimators, a maximum depth of 12, minimum samples per-split at 5 and minimum samples at leaf nodes of 2. Despite the seemingly excessive depth, the mean number of leaf nodes per estimator was around 140 (and never going above 180), due to the regularisation nature of the ensemble method. The chosen configuration was eventually retrained on the entire training/validation dataset and used in the final models.

Probability of BBs under the object model: As in Eq. (5) from the main paper, when the object is presumed hidden ($v_j = \text{Hidden}$), the probability mass function is a Kronecker delta with probability 0 for all detections, and 1 for the hidden BB. It remains to define the parameters of the Gaussian distribution over visible BBs when v_j is Clear or Truncated, which we fit to the training/validation set, but discarding annotations marked as marginal.

We start with defining the means. In the case of the BB centroids, (x, y) , we verified that the mean values per-antenna pickup were largely similar across clear/truncated visibilities. Subsequently, we fit a single model per-antenna. Given that there is limited data for some antennas, we sought to pool information from the geometrical arrangement of neighbouring antennas. To this end, we fit a Homography [4] between the antenna positions on the baseplate (in world-coordinates, as they appear in Fig. 4(b) in main body of the paper), and the corresponding BB annotations (in image-space). The homography construct provides a principled way of sharing statistical strength across the planar arrangement.

On the other hand, inline with our intuition, a Hotelling T2 test [5] on the sizes of the BBs, (w, h) , yielded significant differences (with an 0.01 significance level) between BBs marked as clear or truncated in all but three of the antenna

	Spherical	Pooled Covariance	Per-Visibility
Training LL	-21.97	-21.35	-21.30
Validation LL	-21.83	-21.39	-21.44

Table C.1: Average Log-Likelihoods for Gaussian distribution of BB geometries under different choices of the covariance matrix

positions. Subsequently, we fit individual models per-visibility per-antenna. Again, we find the need to pool samples for statistical strength, and again we leverage the geometry of the cage. Specifically, our belief is that the sizes of the BBs will vary mostly with depth (into the cage) due to perspective, and are largely stable across antennas at the same depth (or conceptual row, in Fig. 4(b)). We thus estimate the mean sizes on a per-‘row’ basis, such that for example, antennas 1, 4, 7, 10, 13 and 16 share the same mean size.

We next discuss estimating the covariance. In actuality, fitting both the Homography on the centroids and the size-means on a per-row/per-visibility basis assumes uniform variance in all directions. However, we investigated computing a more general covariance matrix using the centred data given the ‘means’ inferred from the above step. We explored three scenarios: (a) uniform variance on all dimensions (spherical), (b) full covariance, pooled across antennas and visibilities, and (c) full covariance pooled across antennas but independently per visibility. We fit the statistics on the training set and compared the log-likelihood of the validation-set annotations: Table C.1 shows that option (b) achieved the best scores and was chosen for our weight model.

Probability of BBs under the outlier model: For the general outlier model we fit a Gaussian independently on the centroid, (x, y) and size, (w, h) components. Ideally, we would use a uniform distribution over the size of the image for the former, but in the interest of uniformity with the size-model, we approximate it with a broad Gaussian. The parameters for the sizes are simply estimated on all BB annotations in our training/validation data.

D Description of the Supporting Material

We provide Code and Sample Video Clips at <https://github.com/michael-camilleri/TIM>

D.1 Code

We make available the tracking, identification and evaluation implementations: note that the code is provided as is for research purposes and scrutiny of the algorithm, but is not guaranteed to work without the accompanying setup/frameworks.

- ‘Evaluation.py’: implements the various evaluation metrics,
- ‘Trackers.py’: implementing our changes to the SORT Tracker and packaging it for use with our code,
- ‘Identifiers.py’: implementing the Identification problem and its solution.

D.2 Dataset Sample

Clip 1: This shows a sample video-clip of 30s from our data. The original raw video appears on the left: on the right, we show the same video after being processed with CLAHE [6] to make it more visible to human viewers, together with the RFID-based position of each mouse overlaid as coloured dots. Note that our methods all operate on the raw video and not on the CLAHE-filtered ones.

D.3 Sample Tracking and Identification Videos

We present some illustrative video examples showing the BB tracking each mouse as given by our identification method, and comparisons with other techniques. Apart from the first clip, the videos are played at 5 frames per second (FPS) for clarity, and illustrate the four methods we are comparing in a four-window arrangement with Ours on the top-left, the baseline on the top-right, the static assignment with the probabilistic model bottom-left and the SiamMask tracking bottom-right. The frame number is displayed in the top-right corner of each sub-window. The videos are best viewed by manually stepping through the frames.

Clip 2: We start by showing a minute-long clip of our identifier in action, played at the nominal framerate of 25FPS. This clip illustrates the difficulty of our setup, with the mice interacting with each other in very close proximity (e.g. Blue and Green in frames 42375 – 42570) and often partially/fully occluded by cage elements such as the hopper (e.g. Red in frames 42430 – 42500) or the tunnel (e.g. Blue in frames 42990 – 43020).

Clip 3: This clip shows the ability of our model to handle occlusion. Note for example how in frames 40594 – 40605, the relative arrangement of the RFID tags confuses the baseline (top-right), but the (static) probabilistic weight model is sufficient to reason about the occlusion dynamics and the three mice. Temporal continuity does however add an advantage, as in the subsequent frames, 40607 – 40630, even the static assignment (bottom-left) mis-identifies the mice, mostly due to the lag in the RFID signal. The SiamMask (bottom-right) fails to consistently track any of the mice, mostly because of occlusion and passage through tunnel which happens later on in the video (not shown here), and shows the need for reasoning about occlusions.

Clip 4: This clip shows the weight model successfully filtering out spurious detections. For clarity, we show only the static assignment (left) and the baseline (right). Note how due to a change in the RFID antenna for Green, its BB often gets confused for noisy detections below the hopper (see e.g. frames 40867 – 40875): however, the weight model, and especially the outlier distribution, is able to reject these and assign the correct BB.

Clip 5: This shows another difficult case involving mice interacting and hiding each other. The SiamMask is unable to keep track of any of the mice consistently. While our method does occasionally lose the red mouse when it is severely occluded (e.g. frame 40990) the baseline gets it completely wrong (mis-identifying green for red in e.g. frames 40990 – 41008), mostly due to a lag in the RFID which also trips the static assignment with our weight model.

Clip 6: Finally, this shows an interesting scenario comparing our method (left) to the SiamMask tracker (right). The latter is certainly smoother in terms of the flow of BBs, with the tracking-by-detection approach understandably being more jerky. However, SiamMask’s inability to handle occlusion comes to the fore towards the end of the clip (frames 40693 – end), where the green track latches to the face of the blue mouse.

References

- [1] A. Dutta and A. Zisserman, “The VIA Annotation Software for Images, Audio and Video,” in *Proceedings of the 27th ACM International Conference on Multimedia*, ser. MM ’19. New York, NY, USA: ACM, 2019. [Online]. Available: <https://doi.org/10.1145/3343031.3350535>
- [2] V. V. Vazirani, *Approximation Algorithms*. Springer Berlin Heidelberg, 2003.
- [3] T.-Y. Lin, M. Maire, S. Belongie, J. Hays, P. Perona, D. Ramanan, P. Dollár, and C. L. Zitnick, “Microsoft COCO: Common Objects in Context,” in *Computer Vision – ECCV 2014*, D. Fleet, T. Pajdla, B. Schiele, and T. Tuytelaars, Eds. Cham: Springer International Publishing, 2014, pp. 740–755.
- [4] R. Hartley and A. Zisserman, *Multiple View Geometry in Computer Vision*, 2nd ed. Cambridge, UK: Cambridge University Press, 2004.
- [5] A. V. Alekseyenko, “Multivariate Welch t-test on distances,” *Bioinformatics*, vol. 32, no. 23, pp. 3552–3558, 2016. [Online]. Available: <https://doi.org/10.1093/bioinformatics/btw524>
- [6] K. Zuiderveld, “Contrast limited adaptive histogram equalization,” in *Graphics gems*, P. S. Heckbert, Ed. Academic Press, 1994, pp. 474 – 485.